RSC Advances

PAPER

View Article Online
View Journal | View Issue

Cite this: *RSC Adv.*, 2014, **4**, 30358

Direct electrochemistry of glucose oxidase immobilized on ZrO_2 nanoparticles-decorated reduced graphene oxide sheets for a glucose biosensor†

A. T. Ezhil Vilian,[a] Shen-Ming Chen,*[a] M. Ajmal Ali[b] and Fahad M. A. Al-Hemaid[b]

Received 10th May 2014
Accepted 24th June 2014

DOI: 10.1039/c4ra04350b

www.rsc.org/advances

We fabricated a glucose biosensor based on glucose oxidase (GOx) immobilized in a poly(L-lysine) (PLL) and reduced graphene oxide–zirconium oxide composite (RGO–ZrO_2). First, a simple single step electrochemical approach was used to prepare the RGO–ZrO_2 composite and its successful formation was confirmed by various techniques. Then, a mixture of GOx and PLL was immobilized to form the RGO–ZrO_2 composite. Direct electrochemistry of the GOx was attained for the composite film showing well-defined redox peaks centered at the formal potential −0.403 V. Notably, the peak to peak separation (ΔE_p) was very low (27 mV), while the heterogeneous rate constant for the fast electron transfer was calculated to be 5.03 (±0.14 s^{-1}) revealed. The composite film modified electrode exhibited excellent electrocatalytic ability through the reductive detection of oxygen. A glucose biosensor was developed using the GOx–PLL/RGO–ZrO_2 composite film modified electrode which functioned using differential pulse voltammetry (DPV). The fabricated biosensor exhibited good electrocatalytic ability for the determination of glucose with excellent analytical parameters such as wide linear range of 0.29 mM to 14 mM and high sensitivity of 11.65 (±0.17) μA mM^{-1} cm^{-2}. The sensor results also exhibited appreciable repeatability, reproducibility and stability. Good recovery rates were achieved for the real sample studies proving the promise and practicality of the proposed sensor.

1. Introduction

Graphene is a two-dimensionally arranged carbon nanomaterial that has become a rising star among other carbon nanomaterials due to its exceptional electronic, mechanical and thermal properties.[1–3] Over the past decade, graphene and graphene composites have enjoyed widespread applications in numerous research areas including electronics,[4] supercapacitors,[5] Li-ion batteries,[6] fuel cells,[7] sensors,[8] and biosensors.[9] Chemical oxidation of graphite to graphene oxide (GO) and the subsequent reduction is the most popularly used approach for preparation of a scalable quantity of graphene.[8,10,11] GO, an oxygenated derivative of graphene is the important starting precursor compound for the preparation of graphene-based composites.[12] Notably, GO has a random arrangement of sp^2/sp^3 hybridized carbon atoms with plenty of oxygenated functional groups, which make it highly dispersible in aqueous solutions, whereas graphene does not have oxygen functionalities.[13–15] Recently, numerous efforts have been made to explore the preparation of graphene-based composites with metal nanoparticles,[16] metal oxides,[17] and polymers.[18] Among the aforementioned composites, the graphene–metal oxide composites have drawn considerable attention for use in supercapacitors,[17] solar cells,[19] Li-ion batteries,[20] fuel cells,[21] and sensors.[22,23] Remarkably, the graphene–metal oxide composites exhibit excellent synergistic effects between the graphene and metal oxides.[22]

ZrO_2 is an important transition metal oxide having lower toxicity and higher chemical inertness, which make it more environmentally friendly.[24] In addition, it is highly biocompatible, cheap to produce, thermally stable and electrochemically active.[25,26] Its excellent electrocatalytic properties make it a good candidate for an active electrode material for the electrocatalysis of various important analytes.[26–29] Electrodeposition of ZrO_2 on a self-assembled monolayer template has been used for the fabrication of a modified gold electrode that can be employed for the sensitive determination of parathion.[30] Liu *et al.* developed an electrochemical DNA biosensor based on the incorporation of ZrO_2 in a boron doped diamond modified electrode.[31] Specifically, ZrO_2 has been shown to have good

[a]*Department of Chemical Engineering and Biotechnology, National Taipei University of Technology, No.1, Section 3, Chung-Hsiao East Road, Taipei 106, Taiwan, Republic of China. E-mail: smchen78@ms15.hinet.net; Fax: +886 2270 25238; Tel: +886 2270 17147*

[b]*Department of Botany and Microbiology, College of Science, King Saud University, Riyadh 11451, Saudi Arabia*

† Electronic supplementary information (ESI) available. See DOI: 10.1039/c4ra04350b

potential for the detection of organophosphate pesticides and nerve agents.[25] Recently, Gong *et al.* reported a simple electrochemical method for the fabrication of a ZrO_2 decorated graphene hybrid for the sensing of methyl parathion.[26] Poly(L-lysine) (PLL) is a biocompatible polycationic homopolymer which is very useful in promoting cell adhesion and drug delivery.[32,33] Positively charged PLL has been successfully assembled onto a graphene surface as a linker as a consequence of the formation of the covalent amide group.[34] PLL has drawn substantial attention in the fabrication of biosensors because of its excellent ability to facilitate the transfer of electrons between the biomolecules and the electrode surface.[33] Therefore, in the present work, PLL is used to immobilize glucose oxidase (GOx) onto a graphene–ZrO_2 composite film modified electrode.

Rapid and accurate determination of the blood glucose level is very important from the clinical analysis perspective to control diabetes.[35] Glucose oxidase (GOx) is the most widely employed enzyme to make selective and sensitive glucose biosensors. The GOx enzyme, isolated from *Aspergillus niger*, consists of two identical polypeptide chains each containing FAD/$FADH_2$ as the redox prosthetic group.[35,36] The key to the fabrication of efficient glucose biosensors is the preparation of an appropriate matrix for the immobilization of GOx on the electrode surface.[36] Several successful approaches have been developed over the past years for the immobilization of GOx on various film modified electrodes, such as covalent attachment,[37] electrostatic interactions,[38] and physical adsorption.[39] Some of the reported glucose biosensors include, electro generated magnetic nanoparticles,[40] reduced graphene oxide (RGO)–multiwalled carbon nanotubes (MWCNTs),[9] ZrO_2/Pt–PLL,[41] MWCNT–chitosan/CdSe@CdS composite matrices,[42] sol–gel derived ZrO_2/Nafion composites,[43] reduced graphene oxide (RGO)/ZnO composites,[44] carbon nanotubes (CNTs)/chitosan matrices,[44] gelatin–MWCNTs,[45] nitrogen-doped graphene,[46] and GOx–graphene–chitosan modified electrodes.[47]

In the present study, we fabricate a combined RGO–ZrO_2 composite with PLL which is capable of immobilizing a high amount of GOx and study its direct electrochemistry. The promotion of the direct electron transfer of GOx at the RGO–ZrO_2 modified electrode and its successful application for biosensing indicate that RGO–ZrO_2 could be a good candidate material for the immobilization of biomolecules and the fabrication of a third-generation of biosensors. The function of the fabricated GOx–PLL/RGO–ZrO_2 modified electrode as a biosensor for the sensitive determination of glucose is demonstrated. The electrochemical characteristics and performance of the GOx–PLL/RGO–ZrO_2 modified electrode with respect to the linear range, fast response, low detection limit, high affinity, satisfactory reproducibility and accepted stability are investigated in detail.

2. Experimental procedure

2.1. Apparatus

The electrochemical measurements were carried out using a CHI 405 electrochemical workstation. Electrochemical studies were carried out with a conventional three electrode cell consisting of a modified glassy carbon electrode (GCE) as a working electrode (area 0.071 cm^2), Ag/AgCl (saturated KCl) as a reference electrode and PT wire as a counter electrode. Scanning electron microscopic (SEM) and atomic force microscopic (AFM) characterization were carried out using the S-3000H, Hitachi and CSPM4000, Being Nano-Instruments respectively. Energy-dispersive X-ray (EDX) spectra studies were acquired using the HORIBA EMAX X-ACT (Model 51-ADD0009, Sensor + 24 V = 16 W, resolution at 5.9 keV = 129 eV). The Raman spectra were obtained using the Micro-Raman spectrometer (RENISHAW in the Via system, U.K) with a 514.4 nm He/Ne laser. UV-visible absorption spectroscopy measurements were carried out by using a Hitachi U-3300 spectrophotometer. Powder X-ray diffraction (XRD) studies were performed with an XPERT-PRO (PANalytical B.V., The Netherlands) diffractometer using Cu Kα radiation (k = 1.54 Å). EIM6ex ZAHNER (Kroanch, Germany) was used for the electrochemical impedance spectroscopy (EIS) studies. X-Ray photoelectron spectroscopy (XPS) was carried out using at PHI 5000 Versa Probe equipped with an Al Kalpha X-ray source (1486.6 eV).

2.2. Materials

The zirconyl chloride octahydrate ($ZrOCl_2 \cdot 8H_2O$), graphite (powder, <20 μm), poly-L-lysine (PLL) and glucose oxidase (GOx, from *Aspergillus niger*) were purchased from Sigma Aldrich and used as received. All the reagents were of analytical grade and used without any further purification. All the solutions were prepared using double distilled water. Electrochemical studies were performed with a 0.05 M phosphate buffer solution (PBS) prepared from Na_2HPO_4 and NaH_2PO_4. A stock solution of glucose was prepared in PBS (pH 7) and the solution was kept aside for one day to complete mutarotation.

2.3. Electrochemical fabrication of RGO–ZrO_2 composite modified electrode

Graphite oxide, synthesized from graphite using Hummer's method[48] was then dispersed in water (0.5 mg mL^{-1}) and exfoliated by ultrasonication to produce graphene oxide (GO). Prior to electrode modification, the GCE surface was polished with a 0.05 μm alumina slurry and Buehler polishing cloth before being cleaned well with water. Afterwards, the RGO–ZrO_2 composite for fabrication of the GCE was applied in a single step electrochemical process. Briefly, 5 μL of the GO dispersion was drop cast onto the GCE surface and dried under ambient conditions. The GO modified GCE was then moved to an electrochemical cell containing 5 mM $ZrOCl_2 \cdot 8H_2O$ in PBS (pH 5). In the next step, 10 consecutive cyclic voltammograms (CVs) were recorded in the potential range between 0 and −1.5 V at a scan rate 20 mV s^{-1}. The resulting RGO–ZrO_2 composite film modified GCE was rinsed with water and dried. Then 75 μL of the GOx–PLL mixture (1 : 10) was dropped and spread out onto the surface of the RGO–ZrO_2/GCE and allowed to dry at room temperature. The modified electrode is now the GOx–PLL/RGO–ZrO_2 (Scheme 1). We optimized the amount of PLL and the coverage required to get the maximum GOx redox peak

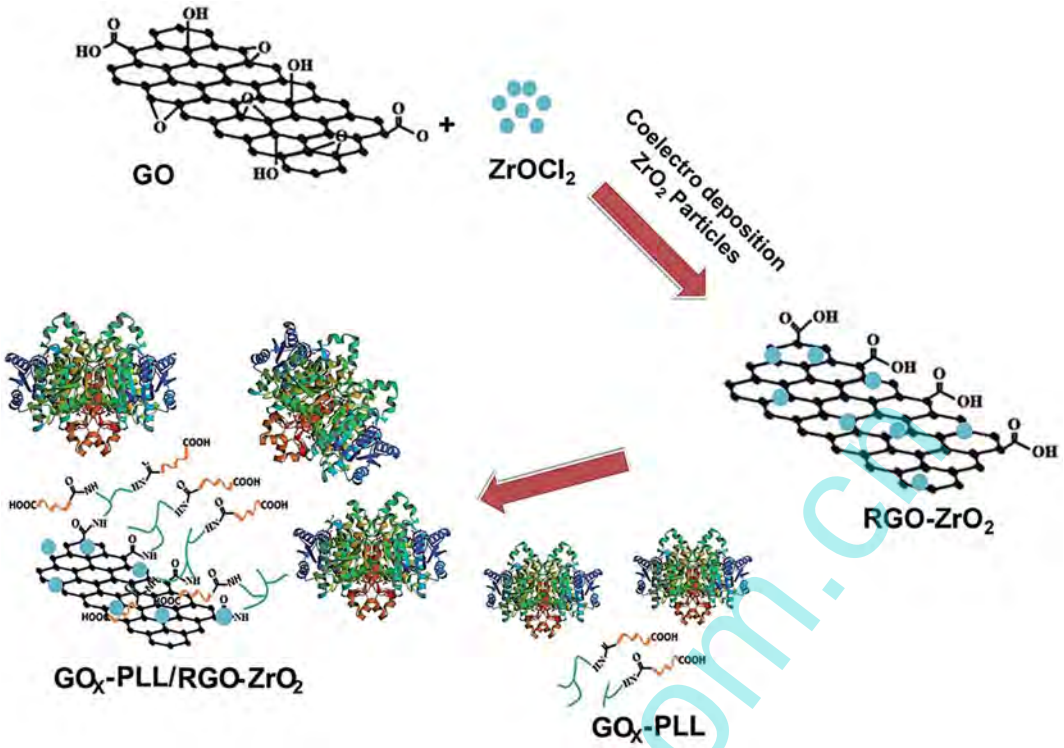

Scheme 1 Schematic representation of the preparation procedure for the GOx–PLL/RGO–ZrO_2 composite.

currents. The maximum redox peak currents were observed when the ratio of GOx to PLL was 1 : 10, so this was the ratio used in subsequent experiments.

3. Results and discussion

3.1. SEM and EDX studies

The SEM image of the GO (Fig. 1A) portrays the characteristic wrinkled, crumpled and sheet like arrangement of GO sheets. The SEM image of ZrO_2 (Fig. 1B) shows a closely assembled network of ZrO_2 particles while the SEM image of RGO–ZrO_2 (Fig. 1C) presents a new morphology with a uniform distribution of numerous ZrO_2 particles on the surface of the RGO sheets with a particle size ranging in a few micrometers. The morphology of the RGO–ZrO_2 composite reveals a uniform decoration of numerous ZrO_2 particles over the entire region of the RGO sheets. The composite has a very good porous structure which can offer a good platform for the immobilization of enzymes or proteins. The SEM image of GOx–PLL/RGO–ZrO_2 (Fig. 1D) shows the complete coverage of RGO–ZrO_2 by GOx–PLL. The amount of GOx immobilized on the modified electrode surface (Γ) is calculated to be 1.57×10^{-10} mol cm^{-2} (calculated in the Section 3.3). The AFM and Raman spectroscopy results also confirmed the successful formation of RGO–ZrO_2 from GO and ZrO_2 (see Fig. S1 and S2†).

The EDX spectrum of GO (Fig. 1E) shows the presence of carbon and oxygen signals with a weight percentage of 54.44 and 45.56% respectively. The oxygen signal reveals the successful formation of GO from graphene. EDX spectra were obtained for the ITO glass and the corresponding signal was deleted for the sake of clarification. The EDX spectrum of ZrO_2 (Fig. 1F) exhibited the signals for zirconium and oxygen with a weight percentage of 35.85 and 64.15%, respectively. The EDX spectrum of RGO–ZrO_2 (Fig. 1G) showed the signals for C, O and Zr with weight percentages of 15.33, 50.72 and 32.95%, respectively. The Zr signals revealed the incorporation of ZrO_2 into the RGO sheets. While the EDX spectrum for the GOx–PLL/RGO–ZrO_2 exhibited the signals indicating the presence of C, O and Zr, with weight percentages of 19.60, 59.59 and 20.81%, respectively (Fig. 1H).

3.2. XRD and XPS studies

The XRD patterns for RGO (a), ZrO_2 (b) and the RGO–ZrO_2 composite (c) are presented in Fig. 2A. The XRD image of RGO shows a broad (0 0 2) diffraction peak at approximately 24.2°, which can be interpreted as disordered stacked graphitic sheets, indicating that the GO has been reduced to RGO, while ZrO_2 exhibits its characteristic diffraction peaks at $2\theta = 30°$, 35°, 38° and 52°. Interestingly, the fact that the RGO–ZrO_2 composite exhibits all the aforementioned diffraction peaks reveals the successful incorporation of ZrO_2 into RGO sheets.[49]

The XPS spectrum of the RGO–ZrO_2 composite shows the presence of the elements of ZrO_2 and carbon (Fig. 2B). The peaks in the wide-scan XPS spectrum of RGO–ZrO_2 (Fig. 2B) correspond to the characteristic peaks of C 1s, O 1s, and Zr 3d, indicating the existence of carbon, oxygen and Zr elements in the sample. This result is consistent with the EDX elemental

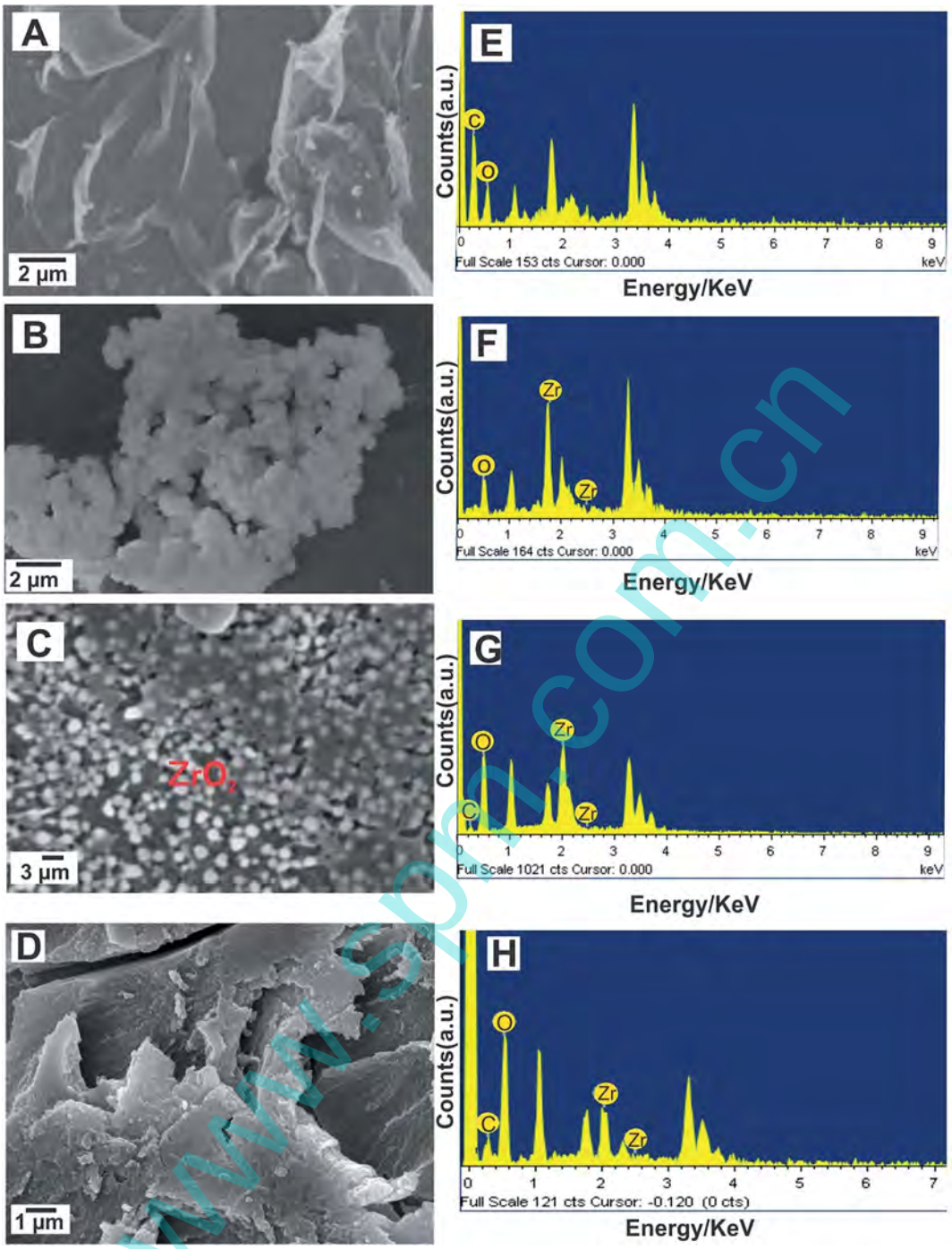

Fig. 1 SEM images of GO (A), ZrO_2 (B), RGO–ZrO_2 (C) and GOx–PLL/RGO–ZrO_2 (D). EDX images of GO (E), ZrO_2 (F), RGO–ZrO_2 (G) and GOx–PLL/RGO–ZrO_2 (H).

analysis. The signal for C 1s obtained at the C=C/C–C (284.5 eV), C–O/C–O–C (hydroxyl and epoxy groups, 286.4 eV), C=O (carbonyl groups, 287.8 eV), and O–C=O (carboxyl groups, 289.0 eV) indicates the presence of graphene sheets (see Fig. 2C), whereas signals corresponding to ZrO_2, such as O 1s, were observed at 532.6. Additionally, the peaks located at 182.8 and 185.4 eV can be attributed to the spin–orbit splitting of the Zr 3d components, Zr $3d_{5/2}$, Zr $3d_{3/2}$ (see Fig. 2E). The binding energy of O 1s in zirconia is located at 530.1 eV. The peak positions and their relative intensities are basically consistent with those for the standard cubic structure of zirconia. It is noted in Fig. 2D that the peaks of Zr 3d and O 1s shift to higher binding energies with increasing particle diameter. Thus, the XPS results also confirm the presence of the various elements in the RGO–ZrO_2 composite[50] and are in good agreement with the XRD results.

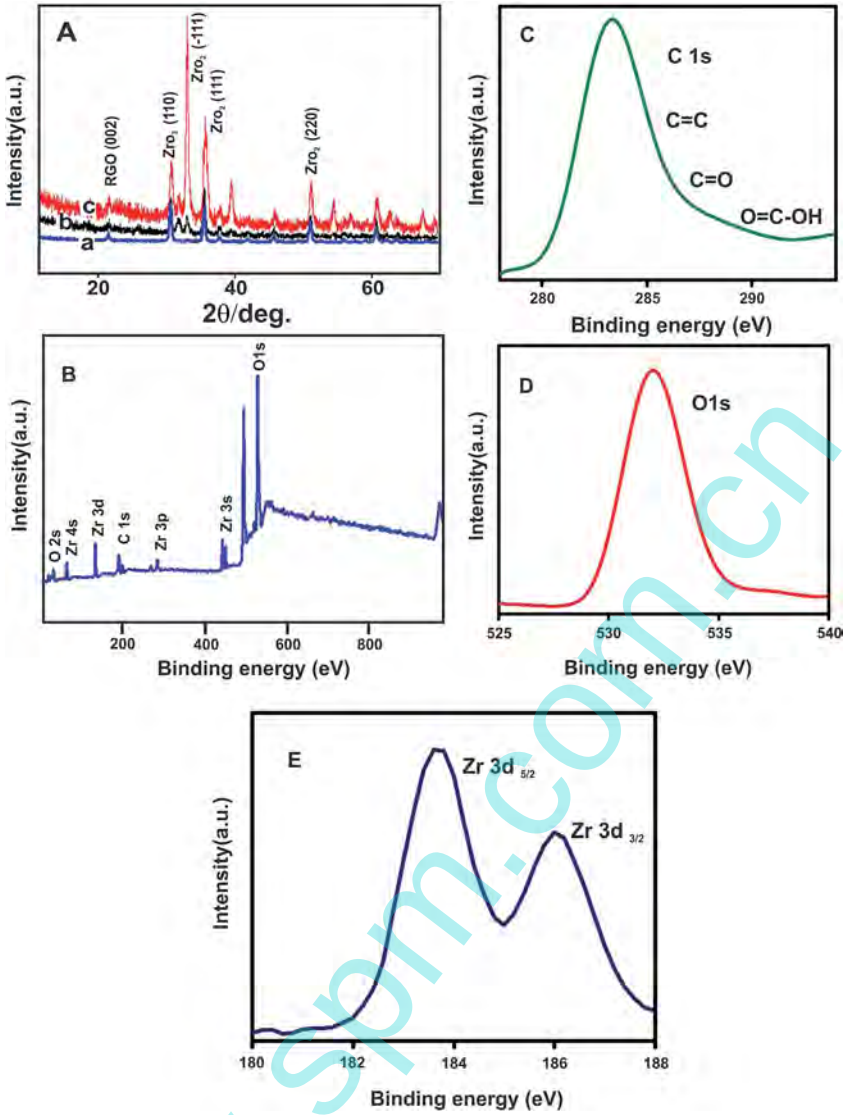

Fig. 2 (A) XRD patterns of RGO (a), ZrO_2 (b) and RGO–ZrO_2 composite (c). (B) XPS spectrum of RGO–ZrO_2 composite, (C) C 1s XPS spectra of RGO–ZrO_2 composite, (D) deconvoluted O 1s spectra of RGO–ZrO_2 composite, (E) Zr 3d core-level spectrum of the RGO–ZrO_2 composite.

3.3. UV-visible spectroscopy and EIS studies

Fig. 3A shows the UV-visible spectrum of GOx and PLL–GOx. The UV-visible spectrum of GOx exhibits two well-defined absorption peaks at 380 and 455 nm which are characteristic of the oxidized form of the FAD group present in GOx. The two peaks exhibited in the UV-visible spectra of PLL–GOx and GOx–PLL/RGO–ZrO_2 are similar in position and shape indicating that the original structural confirmation and native structure of GOx has not been altered during the immobilization process.[51]

EIS experiments were carried out in a PBS (pH 7) containing 5 mM $Fe(CN)_6^{3-/4-}$ as the supporting electrolyte at a potential of 0.5 V *vs.* a saturated Ag/AgCl, in the frequency range between 0.1 Hz to 1 MHz. Fig. 3B shows the real and imaginary parts of the impedance spectra represented as Nyquist plots ($-Z_{im}$ *vs.* Z_{re}) for bare GCE (a), RGO–ZrO_2 (b), GOx/RGO–ZrO_2 (c) and GOx–PLL/RGO–ZrO_2 (d). The impedance values were fitted to the standard Randle's equivalent circuit (see the inset to Fig. 3B) comprised of the charge transfer resistance (R_{et}), ohmic resistance of the electrolyte solution (R_s), Warburg impedance (Z_w) and surface double-layer capacitance (C_{dl}). The semicircles obtained at a lower frequency correspond to a diffusion limited electron-transfer process and those obtained at a higher frequency represent a charge-transfer limited process. The EIS results of the bare GCE showed a semicircular area with R_{et} 554 Ω with decreased in diameter upon modification with RGO–ZrO_2 R_{et} 306 Ω, indicating the increased conductivity at the electrode surface, which can be attributed to the excellent conducting properties of the RGO sheets. The EIS results for the GOx–PLL/RGO–ZrO_2 show a tremendous increase in the diameter of the semicircle and a significant increase of the value of R_{et} to 978 Ω. The increase in the R_{et} value is indicative of increased electrical resistance at the electrode surface due to the insulating bulky protein structure of the GOx. Remarkably, the extent of the increase in the electrical resistance upon GOx

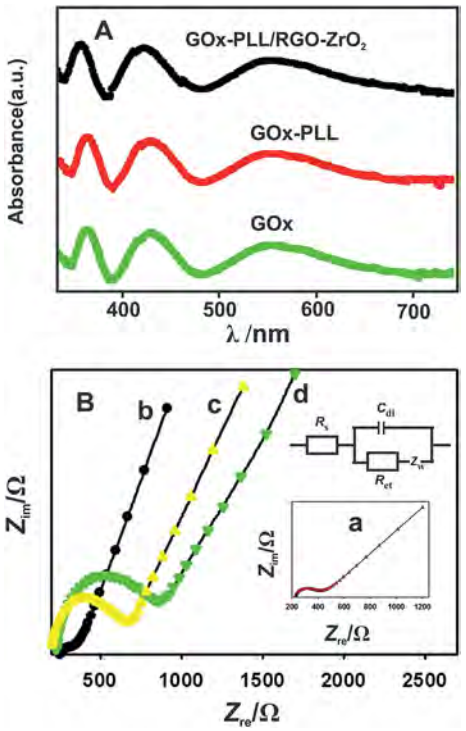

Fig. 3 (A) UV-Vis spectra of GOx, GOx–PLL and GOx–PLL/RGO–ZrO_2. (B) Nyquist plots from EIS results for bare GCE (a), ZrO_2/GCE (b), RGO–ZrO_2/GCE (c), GOx–PLL/RGO–ZrO_2 (d) in PBS (pH 7) containing 5 mM $Fe(CN)_6^{3-/4-}$. Inset: Randles equivalent circuit model.

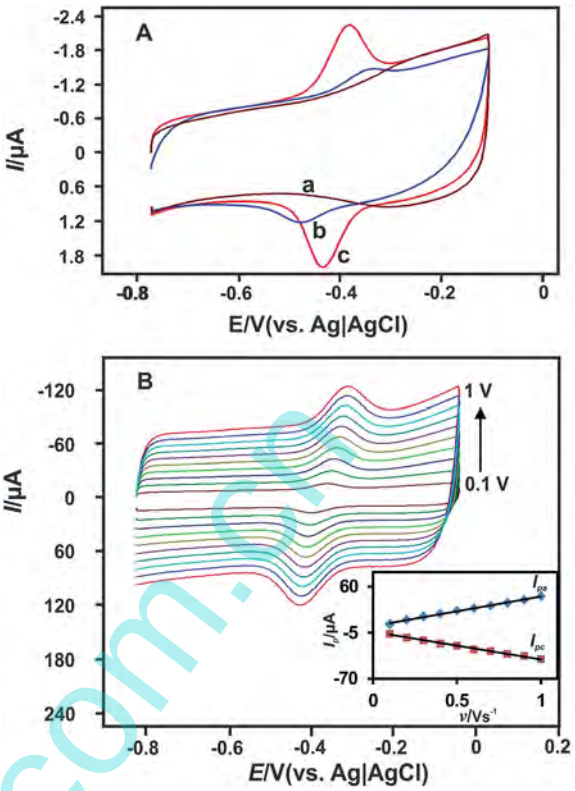

Fig. 4 (A) CVs of bare (a) RGO–ZrO_2 (b) and GOx–PLL/RGO–ZrO_2 (c) film modified GCEs in 0.05 M nitrogen-saturated PBS (pH 7) at the scan rate 50 mV s^{-1}. (B) CVs of GOx–PLL/RGO–ZrO_2 in PBS (pH 7) at the different scan rates from 0.1 to 1 V s^{-1}. Inset: plot of I_{pa} and I_{pc} *versus* scan rates. I_p/μA is presented as a function of ν/V s^{-1}, I_{pa}/μA = 40.83 (±0.38) ν/μA V^{-1} s^{-1} + 4.54 (±0.13)/μA, R^2 = 0.996 and I_{pc}/μA = −38.85 (±0.25) ν/(μA V^{-1} s^{-1}) − 4.016 (±0.14)/μA, R^2 = 0.995 respectively. Error bars represent the standard deviation for 3 independent measurements.

immobilization is a measure of amount of immobilization. An R_{et} of 978 Ω was observed when the GOx was immobilized along with PLL onto the RGO–ZrO_2, whereas an R_{et} of 703 Ω was observed when the GOx was immobilized without PLL. The electrical resistance was higher in the PLL incorporating electrode indicating that PLL plays a significant role towards enabling high GOx loading, a results which is further confirmed by the CV studies discussed in Section 3.2.

3.4. Direct electrochemistry of GOx

The direct electrochemistry of GOx at the GOx–PLL/RGO–ZrO_2/GCE was examined by cyclic voltammetry in N_2 saturated PBS (pH 7) at a scan rate of 50 mV s^{-1} (Fig. 4A). No noteworthy redox peaks were observed for the RGO–ZrO_2/GCE (curve a), whereas a pair of sharp well-defined redox peaks with a formal potential ($E^{\circ\prime}$) of −0.416 V ($FAD/FADH_2$) were observed for the GOx–PLL/RGO–ZrO_2 (curve c). These revealed the direct electron transfer of GOx. The greatly enhanced peak currents and very low peak to peak separation ((ΔE_p) 27 mV) show the fast and efficient electrical communication between the modified electrode surface and the active GOx sites. The large surface area and high conductivity of the composite are the probable reasons for the greatly enhanced direct electrochemical behavior of the GOx. In order to understand the role of PLL, we carried out cyclic voltammetry without the addition of PLL into the electrode matrix. The feeble redox pairs of GOx with $E^{\circ\prime}$ −0.417 V and ΔE_p 125 mV observed at the GOx/RGO–ZrO_2/GCE (curve b) show the lack of efficient electrical communication of the modified electrode with the GOx. On the other hand, the direct electron transfer of GOx was greatly enhanced after the inclusion of PLL into the electrode matrix. This result shows the crucial role of PLL towards promoting electrical communication between the modified electrode surface and the GOx. The stability of the GOx–PLL/RGO–ZrO_2 in PBS (pH 7) was also studied by scanning 500 continuous potentials at a scan rate of 50 mV s^{-1}. It was found that 94.42% of the initial peak current was retained even after 500 continuous cycles, revealing the outstanding stability of the modified film (Fig. S3A†). On the other hand, for the GOx/RGO–ZrO_2/GCE, only about 79.87% of the initial peak current was retained after 500 continuous cycles (Fig. S3B†), showing the poor stability of the electrode without PLL. We also investigated the individual role of RGO and ZrO_2 towards the direct electrochemistry of the GOx and glucose sensors and assessed their special roles (Fig. S4†). On the whole, GOx–PLL/RGO–ZrO_2 has been proved to be an excellent matrix for the direct electrochemistry of GOx, creating a good biocompatible environment for maintaining the bioactivity of the enzyme.

3.5. Effect of scan rate and different pHs

The effect of the scan rate on the redox behavior of GOx in PBS (pH 7) was examined. There was a linear increase in both I_{pa} and I_{pc} as the scan rate increased from 0.1 to 1 V s^{-1} (Fig. 4B). A plot of the peak current *versus* the scan rate reveals a linear relationship which shows that the direct electron transfer of GOx is a surface-controlled process (inset to Fig. 4B). The linear regression equations for the anodic and cathodic process can be expressed as $I_{pa}/\mu A = 40.83\ (\pm 0.38)\nu/\mu A\ V^{-1}\ s^{-1} + 4.54\ (\pm 0.13)/\mu A$, $R^2 = 0.996$ and $I_{pc}/\mu A = -38.85\ (\pm 0.25)\nu/\mu A\ V^{-1}\ s^{-1} - 4.016\ (\pm 0.14)/\mu A$, $R^2 = 0.995$, respectively.

The heterogeneous electron transfer rate constant (k_s) between GOx and the modified electrode was calculated using the Laviron eqn (1).[9] ($n\Delta E_p > 0.200$ V),

$$\log(k_s/s^{-1}) = \alpha \log(1 - \alpha) + (1 - \alpha)\log \alpha - \log[(RT/nFv)(s^{-1})] - \alpha(1 - \alpha)nF\Delta E_p/2.3RT \quad (1)$$

where α is the charge transfer coefficient (calculated to be 0.5 using the Tafel equation),[52] ν is the scan rate in V s^{-1}, n is the number of electrons, and the other parameters R, T and F represent their usual meanings. The k_s value at the GOx–PLL/RGO–ZrO_2 is calculated to be 5.03 s^{-1}, which is comparatively larger than the values reported in the literature, for instance for the MWNT–chitosan/CdSe@CdS composite (1.56 s^{-1}),[42] glucose oxidase–graphene–chitosan (2.83 s^{-1}),[47] or MWNT-coated electrospun gold fibers (1.12 s^{-1}).[53] The comparatively higher k_s value achieved for the GOx–PLL/RGO–ZrO_2 is indicative of the occurrence of rapid electron transfer between the active redox sites for GOx at the modified electrode surface. The amount of electroactive GOx available on the electrode surface (Γ) was calculated to be 1.568×10^{-10} mol cm^{-2}, which is higher than the theoretical monolayer coverage of GOx.[45]

The redox coupling of GOx at the GOx–PLL/RGO–ZrO_2 is confirmed by the stable well-defined and voltammetric redox peaks exhibited over the entire pH range from 1 to 9 (Fig. S6A†). The pH and $E^{\circ\prime}$ (Fig. S6B†) are plotted and who a linear relationship. The respective linear regression equation can be expressed as $E^{\circ\prime}/V = -0.0414\ (\pm 0.51)/V - 0.0578\ (\pm 0.40)$ pH/(V per pH), $R^2 = 0.998$. Here the slope value is −57.8 V per pH, which is close to the theoretical value obtained with the Nernst equation (−58.6 mV per pH) for the transfer process for an equal number of protons and electrons. Thus, the electron transfer process of the FAD/$FADH_2$ redox couples reported in this study involves an equal number of protons and electrons which is consistent with the results reported in the literature.[9,45]

3.6. Determination of glucose

Fig. 5 shows CVs for GOx–PLL/RGO–ZrO_2 in an oxygen saturated PBS (pH 7) for various glucose concentrations obtained after additions of 1 mM (b to e). A sharp voltammetric peak is observed in the presence of glucose at a potential of −0.45 V which is responsible for the electrochemical reduction of oxygen. The reactions occurring at the electrode surface can be explained as follows:

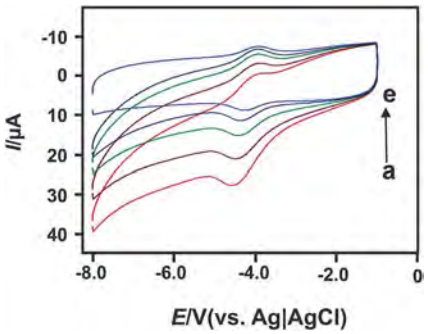

Fig. 5 CVs of GOx–PLL/RGO–ZrO_2 in oxygen saturated PBS (pH 7) containing various concentrations of glucose 0 (a), 1 (b), 1.96 (c), 2.91 (d) and 3.84 mM (e) at a scan rate 50 mV s^{-1}.

$$\text{Glucose} + \text{GOx(FAD)} \rightarrow \text{gluconolactone} + \text{GOx}(FADH_2), \quad (2)$$

$$\text{GOx}(FADH_2) + O_2 \rightarrow \text{GOx(FAD)} + H_2O_2, \quad (3)$$

$$O_2 + 4H^+ + 4e^- \rightarrow 2H_2O. \quad (4)$$

The glucose was oxidized by the GOx to form gluconolactone, while the oxidized form of GOx(FAD) was converted to the reduced form of GOx($FADH_2$) (eqn (2)). Subsequently, the $FADH_2$ was reoxidised to form FAD by consuming oxygen (eqn (3)). Finally the reductive detection of oxygen consumption was monitored at a potential of −0.45 V (eqn (4)). There was a decrease in the peak reduction current responsible for the reduction of oxygen upon addition of the glucose. The linear decrease in the reduction peak current with the consumption of oxygen revealed the efficient electrocatalytic reduction of oxygen at the GOx–PLL/RGO–ZrO_2/GCE. As expected, the GOx–PLL/RGO–ZrO_2/GCE exhibited better electrocatalytic activity for glucose biosensing than the GOx–PLL/ZrO_2/GCE or GOx–PLL/RGO modified GCE (see Fig. S5A and B†). It is known that very high over-potentials are required for the electrocatalytic activity of glucose at the GOx–PLL/ZrO_2/GCE and thus no obvious redox peaks were observed in this electrochemical window (see Fig. S5B†). In comparison with those for the GOx–PLL/ZrO_2/GCE and GOx–PLL/RGO modified GCE, a remarkable decrease in reduction current and positive shift of the peak potential can be observed for the GOx–PLL/RGO modified GCE, however it demonstrated less electrocatalytic activity than that of the GOx–PLL/RGO–ZrO_2/GCE. All these observations indicate the excellent electrocatalytic capability of the GOx–PLL/RGO–ZrO_2/GCE for glucose biosensing (see Fig. 5). We speculate that it was the high surface area of the RGO–ZrO_2 films that increased the capacity for GOx–PLL immobilization, facilitating faster electron-transfer kinetics for glucose biosensing and electrocatalytic activity.

Further, we also investigated the contribution of PLL towards glucose biosensing. Fig. S7(A)† shows the CVs obtained at the GOx/RGO–ZrO_2/GCE (A) in the absence (a) and presence of 3 mM glucose (b) in PBS (pH 7) at a scan rate 50 mV s^{-1}. In the absence of glucose there was a sharp reduction peak observed at

the potential of −0.45 V which can be attributed to the oxygen reduction. No obvious increase in the peak current was observed upon the addition of glucose, indicating that the modified electrode did not have the electrocatalytic ability to sense glucose. Fig. S7(B)† shows the CVs obtained at the GOx–PLL/RGO–ZrO_2 (A) in the absence (a) and presence of 3 mM glucose (b) in PBS (pH 7). A sharp increase in the peak current was observed upon addition of 3 mM of glucose indicating the excellent electrocatalytic ability of the PLL containing modified electrode for glucose biosensing. Thus PLL plays a major role in the GOx–PLL/RGO–ZrO_2 composite towards the determination of glucose.

3.7. Biosensing of glucose at GOx–PLL/RGO–ZrO_2/GCE

Fig. 6A shows the DPVs for the GOx–PLL/RGO–ZrO_2 in an oxygen saturated PBS (pH 7) with various concentrations of glucose. In the absence of glucose, a sharp peak was observed at the potential −0.4 V which can be ascribed to the reduction of oxygen. There was a decrease in the peak current after the addition of 0.29 mM glucose. The peak current decreased linearly upon further addition of glucose indicating the consumption of oxygen after each addition. This could be attributed to the good electrocatalytic ability of the GOx–PLL/RGO–ZrO_2 modified electrode for the efficient reduction of oxygen, which would indirectly assist in the monitoring of the concentration of glucose.

A linear calibration plot was made between the concentration of glucose and the peak current (Fig. 6B). The linear regression equation can be expressed as $I_p(\mu A) = 2.797\ (\pm 0.041) + 100.6\ (\pm 0.072) C_{glucose}$ (mM), $R^2 = 0.992$. The fabricated biosensor exhibited a wide linear range between 0.29 and 14 mM. The sensitivity of the biosensor calculated from the slope of the calibration plot was determined to be 11.65 (±0.17) μA mM^{-1} cm^{-2}. The limit of detection (LOD) was calculated to be 0.13 (±0.021) mM. Here, the LOD was calculated using the formula, LOD = $3s_b/S$, where s_b is the standard deviation of ten blank measurements and S is the sensitivity.[54] The important analytical parameters were compared with those for reported for other sensors available in past studies (Table 1). As can be seen from Table 1, the GOx–PLL/RGO–ZrO_2 offered a quite comparable analytical performance. The results revealed the good capability of the sensor towards the determination of glucose. The DPV technique, which is very sensitive, selective and does not require hydrodynamic conditions as in the case amperometric technique, was used.

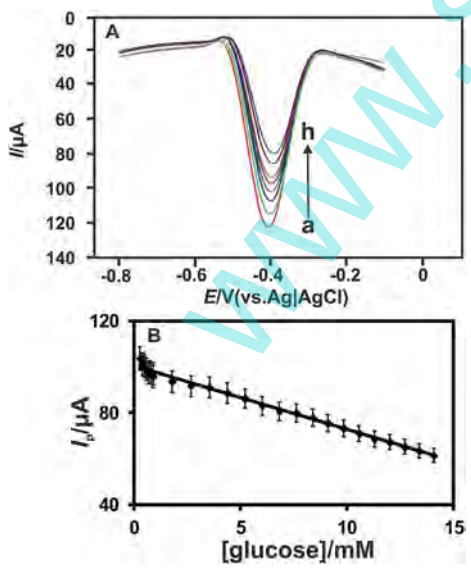

Fig. 6 (A) DPVs of GOx–PLL/RGO–ZrO_2 in oxygen saturated PBS (pH 7) without glucose (a) and with glucose concentrations ranging from 1 to 7 mM (b to h). (B) Plot of response current *vs.* concentration of glucose. $I_p(\mu A) = 2.797\ (\pm 0.041) + 100.6\ (\pm 0.072) C_{glucose}$ (mM), $R^2 = 0.992$. Error bars represent the standard deviation of 3 independent experiments.

3.8. Determination of glucose in urine samples

The practicality of the proposed sensor was also investigated by testing urine samples collected from a diabetes patient. The amount of glucose present in the urine sample was pre-determined by photometric analysis with a ROCHE COBAS C 111 ANALYZER to be 6.423 mM. Then the amount of glucose was also determined using the GOx–PLL/RGO–ZrO_2 modified electrode *via* DPV. The standard addition method was adopted to calculate the concentration of glucose and it was found to be 6.744 mM, a result which is in good agreement with the photometric analysis. This confirms that the proposed sensor can be useful for the determination of glucose present in human urine samples.

Next, urine samples collected from a healthy man were diluted in 0.1 M PBS at a ratio of 1 : 100. Known concentrations of glucose samples were spiked into the urine samples which were analyzed using the GOx–PLL/RGO–ZrO_2/GCE (Fig. S8†). Fig. S8† presents the CVs obtained for the GOx–PLL/RGO–ZrO_2/GCE for urine samples without (a) with 1 mM (b), 2 mM (c), 3 mM (d) and 4 mM glucose (e); the scan rate was 50 mV s^{-1}. Recovery rates were calculated from the CV results. Comparison of the values for the spiked samples and determined samples exhibited good recoveries from 97 to 102.5%, as shown in Table S1.† Good recoveries achieved for the determination of glucose in the spiked human urine samples revealed the practicality of the proposed biosensor.

3.9. Stability, repeatability and reproducibility studies

The repeatability of using the same GOx–PLL/RGO–ZrO_2 modified electrode was examined. In the tests we used 1 mM of glucose in a 0.1 M pH 7.0 PBS. Results showed that the relative standard deviation for 5 determinations was 2.57% (see Fig. S9†). In addition, the relative standard deviation of the current signals for measurement of 1 mM glucose in 0.1 M pH 7.0 PBS for 6 independently prepared biosensors was determined to be 2.6%, which proves the good reproducibility of the biosensor preparation process (see Fig. S10†). On the other hand, the long-term stability of the proposed biosensor was also estimated by measuring its response to a 1 mM glucose solution after the electrode had been stored in a dry state at 4 °C for 1 month. The biosensor retained 94.4% of its original response

Table 1 Comparison of the electroanalytical parameters of the GOx–PLL/RGO–ZrO_2 with other GOx-based modified electrodes

Electrode	Method	Linear range/mM	Sensitivity μA mM^{-1} cm^{-2}	Ref.
GOx–PMB[a]@$SiO_{2(nano)}$	DPV	0.01–1.11	—	55
GOx/(SiO_2–PA[b])	DPV	0.016–8	—	56
GOx/colloidal Au	CV	0.04–0.28	8.4	57
PDDA[c]–GOx/Au/CNT	Amperometry	0.5–5.0	2.5	58
OOPPy[d]–nanoAu/GOx	Amperometry	1–8	—	59
GOx/SnS_2/Nafion/GCE	Amperometry	0.025–1.1	7.6	60
GOx/Pt/FCNA[e]/GCE	Amperometry	0.5–8.0	6.0	61
Nafion/GOx/Ag/Pdop[f]@CNT/GCE	Amperometry	0.05–1.1	3.1	62
RGO/Ag/GOx	CV	0.5–12.5	3.84	63
GOx–PLL/RGO–ZrO_2	DPV	0.29–14	11.65 (±0.17)	Our work

[a] Poly(methylene blue). [b] Phytic acid. [c] Poly(diallyldimethylammonium chloride). [d] Overoxidized polypyrrole. [e] Flower-like carbon nanosheet aggregation. [f] Polydopamine.

after 1 month, which proves that the RGO–ZrO_2 efficiently maintained the activity of GOx (see Fig. S11†). The appreciable stability, repeatability and reproducibility results achieved indicate that the GOx–PLL/RGO–ZrO_2 modified electrode based sensor is a versatile sensor for the determination of glucose.

4. Conclusion

A GOx–PLL/RGO–ZrO_2 modified electrode was prepared by a simple electrochemical process. The direct electrochemistry of the GOx showed greatly enhanced redox peak currents and fast electron transfer constants. The modified electrode exhibited excellent electrocatalytic ability towards the determination of glucose by the reductive detection of oxygen. The developed biosensor exhibited good analytical parameters for efficient glucose determination by the DPV technique. In addition, the sensor offered good repeatability, reproducibility and stability results. The excellent performances of the prepared composite film can also be explored for the immobilization of other redox enzymes or proteins.

Acknowledgements

Research supported by the King Saud University, Deanship of Scientific Research, College of Science, Research Center.

References

1 V. Singh, D. Joung, L. Zhai, S. Das, S. I. Khondaker and S. Seal, *Prog. Mater. Sci.*, 2011, **56**, 1178–1271.
2 A. K. Geim, *Science*, 2009, **324**, 1530–1534.
3 Y. Dong, H. Pang, H. B. Yang, C. Guo, J. Shao, Y. Chi, C. M. Li and T. Yu, *Angew. Chem., Int. Ed.*, 2013, **30**, 7800–7804.
4 X. Wu, M. Sprinkle, X. Li, F. Ming, C. Berger and W. A. D Heer, *Phys. Rev. Lett.*, 2008, **101**, 026801.
5 J. J. Yoo, K. Balakrishnan, J. Huang, V. Meunier, B. G. Sumpter, A. Srivastava, M. Conway, A. L. M. Reddy, J. Yu, R. Vajtai and P. M. Ajayan, *Nano Lett.*, 2011, **11**, 1423–1427.
6 S. Yang, G. Cui, S. Pang, Q. Cao, U. Kolb, X. Feng, J. Maier and K. Mullen, *ChemSusChem*, 2010, **3**, 236–239.
7 C. X. Guo, L. Y. Zhang, J. Miao, J. Zhang and C. M. Li, *Adv. Energy Mater.*, 2013, **3**, 167–171.
8 V. Mani, A. P. Periasamy and S. M. Chen, *Electrochem. Commun.*, 2012, **17**, 75–78.
9 V. Mani, B. Devadas and S. M. Chen, *Biosens. Bioelectron.*, 2013, **41**, 309–315.
10 M. Pumera, A. Ambrosi, A. Bonanni, E. L. K. Chng and H. L. Poh, *TrAC, Trends Anal. Chem.*, 2010, **29**, 954–965.
11 S. Park, J. An, J. R. Potts, A. Velamakanni, S. Murali and R. S. Ruoff, *Carbon*, 2011, **49**, 3019–3023.
12 D. Chen, H. Feng and J. Li, *Chem. Rev.*, 2012, **112**, 6027–6053.
13 S. Kim, S. Zhou, Y. Hu, M. Acik, Y. J. Chabal, C. Berger, W. Heer, A. Bongiorno and E. Riedo, *Nat. Mater.*, 2012, **11**, 544–549.
14 S. Stankovich, R. Piner, S. T. Nguyen and R. S. Ruoff, *Carbon*, 2006, **44**, 3342–3347.
15 Z. B. Liu, Y. F. Xu, X. Y. Zhang, X. L. Zhang, Y. S. Chen and J. G. Tian, *J. Phys. Chem. B*, 2009, **113**, 9681–9686.
16 Q. Zhuo, Y. Ma, J. Gao, P. Zhang, Y. Xia, Y. Tian, X. Sun, J. Zhong and X. Sun, *Inorg. Chem.*, 2013, **52**, 3141–3147.
17 S. Chen, J. Zhu, X. Wu, Q. Han and X. Wang, *ACS Nano*, 2010, **4**, 2822–2830.
18 Y. Sun and G. Shi, *J. Polym. Sci., Part B: Polym. Phys.*, 2013, **51**, 231–253.
19 S. Sun, L. Gao and Y. Liu, *Appl. Phys. Lett.*, 2010, **96**, 083113.
20 G. Wang, J. Liu, S. Tang, H. Li and D. Cao, *J. Solid State Electrochem.*, 2011, **15**, 2587–2592.
21 Y. Liang, Y. Li, H. Wang, J. Zhou, J. Wang, T. Regier and H. Dai, *Nat. Mater.*, 2011, **10**, 780–786.
22 G. Singh, A. Choudhary, D. Haranath, A. G. Joshi, N. Singh, S. Singh and R. Pasricha, *Carbon*, 2012, **50**, 385–394.
23 L. Peng, X. Peng, B. Liu, C. Wu, Y. Xie and G. Yu, *Nano Lett.*, 2013, **13**, 2151–2157.
24 B. Liu, J. Hu and J. S. Foord, *Electrochem. Solid-State Lett.*, 2011, **14**, D20–D22.
25 G. Liu and Y. Lin, *Anal. Chem.*, 2005, **77**, 5894–5901.
26 J. Gong, X. Miao, H. Wan and D. Song, *Sens. Actuators, B*, 2012, **162**, 341–347.

27 W. Sun, X. Wang, Xi. Sun, Y. Deng, J. Liu, B. Lei and Z. Sun, *Biosens. Bioelectron.*, 2013, **44**, 146–151.
28 M. Das, C. Dhand, G. Sumana, A. K. Srivastava, R. Nagarajan, L. Nain, M. Iwamoto, T. Manaka and B. D. Malhotra, *Biomacromolecules*, 2011, **12**, 540–547.
29 Z. Tong, R. Yuan, Y. Chai, S. Chen and Y. Xie, *Biotechnol. Lett.*, 2007, **29**, 791–795.
30 J. H. Zhou, C. Y. Deng, S. H. Si and S. E. Wang, *Microchim. Acta*, 2011, **172**, 207–215.
31 B. Liu, J. Hu and J. S. Foord, *Electrochem. Commun.*, 2012, **19**, 46–49.
32 S. Some, S. M. Ho, P. Dua, E. Hwang, Y. H. Shin, H. J. Yoo, J. S. Kang, D. K. Lee and H. Lee, *ACS Nano*, 2012, **6**, 7151–7161.
33 C. Shan, H. Yang, D. Han, Q. Zhang, A. Ivaska and L. Niu, *Langmuir*, 2009, **25**, 12030–12033.
34 D. Zhang, Y. Zhang, L. Zheng, Y. Zhan and L. He, *Biosens. Bioelectron.*, 2013, **42**, 112–118.
35 C. X. Guo and C. M. Li, *Phys. Chem. Chem. Phys.*, 2010, **12**, 12153–12159.
36 Z. Luo, L. Yuwen, Y. Han, J. Tian, X. Zhu, L. Weng and L. Wang, *Biosens. Bioelectron.*, 2012, **36**, 179–185.
37 S. Zhang, N. Wang, H. Yu, Y. Niu and C. Sun, *Bioelectrochemistry*, 2005, **67**, 15–22.
38 Z. Ma and T. Ding, *Nanoscale Res. Lett.*, 2009, **4**, 1236–1240.
39 W. Z. Jia, K. Wang, Z. J. Zhu, H. T. Song and X. H. Xia, *Langmuir*, 2007, **23**, 11896–11900.
40 F. N. Comba, M. D. Rubianes, L. Cabrera, S. Gutierrez, P. Herrasti and G. A. Rivasa, *Electroanalysis*, 2010, **22**, 1566–1572.
41 X. Yang, Q. Zhang, Y. Sun and S. Liu, *IEEE Sens. J.*, 2007, **7**, 1735–1741.
42 F. Huang, F. Wang, S. Feng, Y. Li, S. Li and Y. Li, *J. Solid State Electrochem.*, 2013, **17**, 1295–1301.
43 H. J. Kim, S. H. Yoon, H. N. Choi, Y. K. Lyu and W. Y. Lee, *Bull. Korean Chem. Soc.*, 2006, **27**, 65–70.
44 Y. Liu, M. Wang, F. Zhao, Z. Xu and S. Dong, *Biosens. Bioelectron.*, 2005, **21**, 984–988.
45 A. P. Periasamy, Y. J. Chang and S. M. Chen, *Bioelectrochemistry*, 2011, **80**, 14–120.
46 Y. Wang, Y. Shao, D. W. Matson, J. Li and Y. Lin, *ACS Nano*, 2010, **4**, 1790–1798.
47 X. Kang, J. Wang, H. Wu, I. A. Aksay, J. Liu and Y. Lin, *Biosens. Bioelectron.*, 2009, **25**, 901–905.
48 W. S. Hummers and R. E. Offeman, *J. Am. Chem. Soc.*, 1958, **80**, 1339.
49 C. J. Cai, M. W. Xu, S. J. Bao, C. Lei and D. Z. Jia, *RSC Adv.*, 2012, **2**, 8172–8178.
50 M. Niasari, M. Dadkhah and F. Davar, *Polyhedron*, 2009, **28**, 3005–3009.
51 H. Liu and N. Hu, *Electroanalysis*, 2007, **19**, 884–892.
52 A. J. Bard and L. R. Faulkner, *Electrochemical Methods: Fundamentals and Applications,*Wiley, New York, 2nd edn, 2001.
53 M. V. Jose, S. Marx, H. Murata, R. R. Koepsel and A. J. Russell, *Carbon*, 2012, **50**, 4010–4020.
54 A. Radoi, D. Compagnone, E. Devic and G. Palleschi, *Sens. Actuators, B*, 2007, **121**, 501–506.
55 X. Xiao, B. Zhou, L. Zhu, L. Xu, L. Tan, H. Tang, Y. Zhang, Q. Xie and S. Yao, *Sens. Actuators, B*, 2012, **165**, 126–132.
56 W. Zhao, Y. Ni, Q. Zhu, R. Fu, X. Huang and J. Shen, *Biosens. Bioelectron.*, 2013, **44**, 1–5.
57 S. Liu and H. Ju, *Biosens. Bioelectron.*, 2003, **19**, 177–183.
58 Y. L. Yao and K. K. Shiu, *Electroanalysis*, 2008, **20**, 1542–1548.
59 B. Haghighi and M. A. Tabrizi, *Colloids Surf., B*, 2013, **103**, 566–571.
60 Z. J. Yang, Y. Y. Ren, Y. C. Zhang, J. Li, H. B. Li, X. C. Huang, X. Y. Hu and Q. Xu, *Biosens. Bioelectron.*, 2011, **26**, 4337–4341.
61 S. Tang, X. Z. Wang, J. P. Lei, Z. Hu, S. Y. Deng and H. X. Ju, *Biosens. Bioelectron.*, 2010, **26**, 432–436.
62 Y. L. Wang, L. Liu, M. G. Li, S. D. Xu and F. Gao, *Biosens. Bioelectron.*, 2011, **30**, 107–111.
63 S. Palanisamy, C. Karuppiah and S. Chen, *Colloids Surf., B*, 2014, **114**, 164–169.